hv photonics

IMPACT FACTOR 2.1

CITESCORE 2.6

Article

Determination of the XUV Frequency Chirp at the Free-Electron Laser FLASH via THz Streaking and Electron Beam Diagnostics

Mahdi M. Bidhendi, Gesa Goetzke, Ivette J. Bermudez Macias, Rosen Ivanov, Evgeny A. Schneidmiller, Najmeh Mirian and Stefan Düsterer

Special Issue

From Theory to Reality: Progress and Challenges in Free-Electron Laser Development

Edited by

Dr. Najmeh Mirian

MDPI

https://doi.org/10.3390/photonics11121153

photonics

MDPI

Article

Determination of the XUV Frequency Chirp at the Free-Electron Laser FLASH via THz Streaking and Electron Beam Diagnostics

Mahdi M. Bidhendi *, Gesa Goetzke, Ivette J. Bermudez Macias †, Rosen Ivanov †, Evgeny A. Schneidmiller, Najmeh Mirian ‡ and Stefan Düsterer

Deutsches Elektronen-Synchrotron DESY, Notkestr. 85, 22607 Hamburg, Germany; gesa.goetzke@desy.de (G.G.); ivette.bermudez@xfel.eu (I.J.B.M.); rosen.ivanov@xfel.eu (R.I.); evgeny.schneidmiller@desy.de (E.A.S.); mirian81@hzdr.de (N.M.); stefan.duesterer@desy.de (S.D.)

* Correspondence: mahdi.mohammadi-bidhendi@desy.de

† Current address: European XFEL GmbH, Holzkoppel 4, 22869 Schenefeld, Germany.

‡ Current address: Helmholtz-Zentrum Dresden-Rossendorf, Bautzner Landstr. 400, 01328 Dresden, Germany.

Abstract: Free-electron lasers (FELs) operating in the extreme ultraviolet (XUV) and X-ray regions deliver ultrashort pulses with unprecedented intensity, enabling groundbreaking research across various scientific disciplines. A potential chirp (frequency change within the pulse) of these pulses influences their spectral properties, directly impacting the experimental outcomes and FEL performance. The accurate characterization of the chirp is, therefore, important for optimizing FEL operation and interpreting experimental results. This study presents a comprehensive comparison of two techniques determining the chirp of the XUV pulses at FLASH by directly measuring the XUV pulses with THz streaking and by detecting the chirp of the electron bunches by a Transverse Deflection Structure (PolariX TDS) to infer the XUV chirp. We conducted simultaneous measurements using both techniques at FLASH2 while tuning the FEL to produce various energy chirps on the electron bunch.

Keywords: free-electron lasers; temporal diagnostic; XUV pulses; SASE; THz streaking

Citation: Bidhendi, M.M.; Goetzke, G.; Bermudez Macias, I.J.; Ivanov, R.; Schneidmiller, E.A.; Mirian, N.; Düsterer, S. Determination of the XUV Frequency Chirp at the Free-Electron Laser FLASH via THz Streaking and Electron Beam Diagnostics. *Photonics* **2024**, *11*, 1153. https://doi.org/10.3390/photonics11121153

Received: 5 November 2024
Revised: 4 December 2024
Accepted: 5 December 2024
Published: 7 December 2024

1. Introduction

Free-electron lasers (FELs) operating in the extreme ultraviolet (XUV) and X-ray regions deliver photon pulses with femtosecond (fs) durations and unparalleled intensity. These pulses typically range from several hundred femtoseconds down to just a few femtoseconds, with photon counts between 10^{11} and 10^{13} per pulse [1–6]. Most XUV and X-ray FELs operate in the self-amplified spontaneous emission (SASE) regime, resulting in each pulse exhibiting a unique combination of pulse energy, XUV spectrum, arrival time, pulse duration, and chirp. Therefore, it is critical to perform temporal characterization of the pulses on a shot-by-shot basis for proper interpretation of the experimental data.

Traditional photodetectors lack the necessary response time to operate in the few-femtosecond regime, and time–frequency correlation techniques commonly used in the optical domain are difficult to implement due to the small cross-sections in nonlinear processes at X-ray wavelengths. This necessitates the development of advanced methods for single-shot temporal characterization of FEL pulses.

Several diagnostic techniques have been devised to study the temporal properties of FEL pulses [7]. One effective method for single-shot characterization is the THz streaking technique, which is typically used to measure the pulse duration of the XUV pulses [8–10]. However, by extending the technique, one can infer the linear part of the frequency chirp across the XUV pulses [8,11,12].

Another complementary approach involves measuring the longitudinal phase space of the electron bunch, producing the XUV SASE radiation, using an X-Band Transverse Deflection Structure (PolariX TDS) [13,14]. The PolariX TDS, in combination with an

electron beam energy spectrometer, can be used to determine the time–energy distribution of the electron bunches. In addition, the setup allows for determining which part of the electron bunch contributed to the XUV SASE pulse [15] and, thus, allows for estimating a possible frequency chirp of the XUV pulse.

In FEL experiments, usually a potential chirp is not considered as an important parameter, while the analysis of previous THz streaking and TDS data shows that the XUV pulses at FLASH are typically chirped. For many applications, the influence of chirp is rather small, while it can influence other areas noticeably, for example, in femto-chemistry where the chirp can even be used to alter the pathway of the chemical reactions [16–18]. Another consequence of a chirped electron bunch is a broader bandwidth of the XUV pulse. By tilting the electron bunch in the time–energy domain, additional electron energies contribute to the lasing process, leading to a broader XUV spectrum. Looking, e.g., for absorption spectroscopy [19–21] or X-ray crystallography [22], a broad spectrum allows for covering larger ranges of spectral lines or diffraction patterns in a single FEL pulse without lengthy scanning of the FEL wavelength and, thus, speeding up data acquisition. Here, a chirp is rather advantageous.

In this paper, we focus on measuring the linear chirp of the XUV pulses from FLASH2 [23], using THz streaking and PolariX TDS as the only two diagnostic techniques at FLASH, which are potentially able to determine the chirp. Each method offers unique advantages for characterizing the temporal properties of XUV pulses. By comparing these techniques, we aim to provide comprehensive insights into their effectiveness and applicability to optimize the FEL performance and interpret the experimental results.

2. Experimental Techniques

2.1. THz Streaking

To determine the pulse duration and linear part of the chirp of the XUV FEL pulses, we employed the THz streaking technique [8,9]. This method involves using a noble gas target photoionized by the FEL pulses. The resulting photoelectrons carry the temporal and spectral properties of the ionizing XUV radiation. As these photoelectrons propagate through the time-varying electric field of the co-propagating THz radiation, their kinetic energy distribution is influenced by the field. This distribution is then measured by an electron time-of-flight (eTOF) spectrometer.

The momentum component of the photoelectrons changes depending on the time of ionization relative to the THz field. If the electron wave packet is short compared with the period length of the THz field, the temporal structure of the electron wave packet is mapped onto the kinetic energy distribution of the emitted photoelectrons, allowing for the determination of the pulse duration and linear chirp [11].

The THz streaking setup featured an interaction chamber where the XUV and THz beams were focused co-linearly at the interaction point [24]. This point was monitored by two eTOFs positioned opposite each other, perpendicular to the propagation direction of the XUV pulses, as shown in Figure 1a. The second eTOF was installed to allow the simultaneous measurement of photoelectrons created by the XUV FEL pulse interacting with the same THz field, but with opposite momentum shifts. A dedicated laser system provided ∼1 ps long pulses at 1030 nm, with a pulse energy of ∼3.5 mJ and a repetition rate of 10 Hz. These laser pulses generate THz radiation through optical rectification using a nonlinear crystal ($LiNbO_3$). Details can be found in the following references [10,24,25].

By varying the delay between the THz field and the XUV pulse, the photoelectron spectra (often called "streaking trace") are recorded, which represent the vector potential A_{streak} of the THz field [11]. As the THz field is polarized in the plane of the two eTOFs, one eTOF records an upshift in the energy, while the other measures a reduced energy. The streaking traces for both eTOFs are shown in Figure 1b. The "first" slope corresponds to the initial interaction of the THz field with photoelectrons, while the "second" slope follows as the THz field continues interacting with the photoelectrons, as illustrated in Figure 1b. In this setup, the photoelectrons are streaked by a large fraction of the THz pulse.

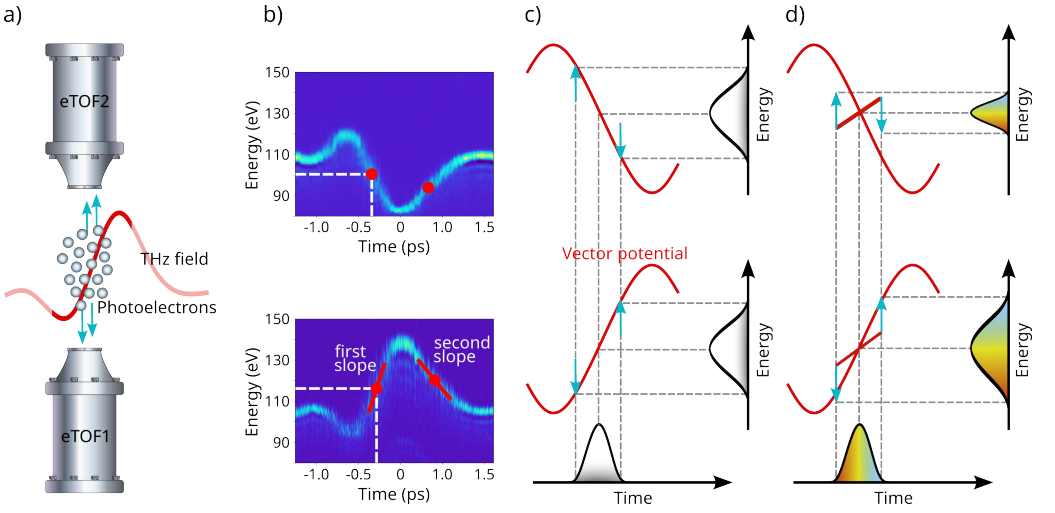

Figure 1. (**a**) Schematic representation of the chirp measurement using the THz streaking setup. Photoelectrons are generated due to the photoionization of gas atoms by the XUV FEL pulse. The kinetic energy of the photoelectrons is modified by the THz field and subsequently measured by eTOF1 and eTOF2. (**b**) The photoelectron spectra (Neon 2p line) for eTOF1 (bottom) and eTOF2 (top) are shown as the a delay scan of the THz field leading to the so-called "streaking trace", which is proportional to the vector potential of the THz field. The red lines show the so-called "first" and "second" slope of the streaking field, and red points indicate the delay value between the FEL and THz pulse of the middle of the linear part of the streaking trace where the streaking data are measured. (**c**) Mapping the temporal information of an unchirped XUV pulse onto the kinetic energy distribution of photoelectrons. The spectral broadening measured by both eTOFs is identical, indicating zero XUV chirp. (**d**) Mapping the temporal information of a negative linearly chirped XUV pulse (higher energy at the head of the pulse represented as blue and lower energy later represented as red) onto the kinetic energy distribution of photoelectrons. For the spectrum measured by eTOF1 (bottom row), the XUV chirp accelerates the fast photoelectrons further and decelerates the slower ones more, resulting in a larger spectral broadening compared with an unchirped XUV pulse. In contrast, for the spectrum measured by eTOF2, the chirp counteracts the streaking field by decelerating the fast photoelectrons and accelerating the slower ones, leading to reduced spectral broadening.

The difference between the up- and down-shifted streaking spectra yields information to determine the linear part of the chirp of the XUV pulse [11]. Setting the delay between the XUV pulse and the streaking field to the center of the linear part of the THz field (red dot in Figure 1b, the slope of A_{streak} is positive for eTOF1 and negative for eTOF2. As illustrated in Figure 1c, the width of the streaked spectrum remains unaffected by the sign of the streaking field for a pulse with no XUV chirp. This results in identical spectral broadening measured by both eTOFs. Thus, the actual pulse duration can easily be determined as $\tau_{XUV} = \sqrt{\sigma_{\mathrm{TOF}}^2 - \sigma_{\mathrm{ref}}^2} \big/ s_{\mathrm{TOF}}$, where σ_{TOF} is the spectral width measured by eTOF1 or eTOF2, σ_{ref} is the spectral width of the unstreaked photoelectrons, and s_{TOF} is the slope of the THz field or the so-called streaking speed, which is calculated by fitting the linear part of the streaking trace as shown in Figure 1b.

In contrast, for a linearly chirped XUV pulse, as shown in Figure 1d the "induced" chirp of the streaking field and the inherent XUV chirp add up or counteract. In the shown case for a negatively chirped XUV pulse (high-energy photoelectrons at the head and low-energy at the tail), the faster electrons generated at the beginning of the pulse are decelerated, while the slower electrons generated at the end of the pulse are accelerated for eTOF2. This causes eTOF2 to measure a streaked spectrum that is narrower than that of an unchirped XUV pulse, whereas eTOF1 records a broader streaked spectrum. This difference can be used to determine a linear approximation of the chirp of XUV pulses, while higher orders of the chirp can unfortunately not be reliably reconstructed with this method. This, however, also implies that in the case of a chirped XUV pulse, the different broadening

of the streaked spectra leads to a more complicated determination of the pulse duration. Under certain conditions, more advanced techniques capable of measuring higher-order chirp can be employed to overcome these limitations, as discussed in [26].

In the streaking trace shown in Figure 1b, we observed that the energy of photoelectrons measured at the center of the linear slopes on eTOF1 and eTOF2 differ slightly (red dots in Figure 1b). In addition, due to the asymmetric shape of the THz field, the streaking speeds at the first and second slope are different. Therefore, the spectral broadening measured on the first and second slopes of the THz field for a single eTOF differs. To account for these differences, the streaking speed and reference width are determined for each eTOF independently, leading to Equations (1) and (2). Assuming that the streaked spectrum maintains a Gaussian shape, the XUV pulse duration can be written as [12]:

$$\tau_{XUV} = \sqrt{\frac{(\sigma_1^2 - \sigma_{\mathrm{ref},1}^2)s_2 + (\sigma_2^2 - \sigma_{\mathrm{ref},2}^2)s_1}{(s_1 + s_2)s_1 s_2}}, \tag{1}$$

where σ_1 and σ_2 are the spectral widths measured by eTOF1 and eTOF2 consecutively, $\sigma_{\mathrm{ref},1}$ and $\sigma_{\mathrm{ref},2}$ are the spectral widths measured in the absence of the streaking field with eTOF1 and eTOF2, respectively. s_1 and s_2 are the streaking speeds measured by eTOF1 and eTOF2, respecitvely. In addition, the difference in the streaked widths can be used to obtain information about the linear part of the XUV chirp:

$$c = \frac{(\sigma_1^2 - \sigma_{\mathrm{ref},1}^2)s_2^2 - (\sigma_2^2 - \sigma_{\mathrm{ref},2}^2)s_1^2}{4s_1 s_2 (s_1 + s_2)\tau_{XUV}^2}. \tag{2}$$

Here, two eTOFs provide the invaluable advantage that the needed two measurements can be acquired simultaneously for each streaked FEL pulse. If only one eTOF is available, one still could obtain an estimate of the chirp and the correct pulse duration, when one measures sequentially the broadening on the first slope and then on the second slope (see Figure 1b and Ref. [12]).

2.2. PolariX TDS

The PolariX TDS [27,28], installed downstream of the undulators at FLASH2, offers direct access to the longitudinal and energy distribution of electron bunches. The setup consists of an X-band RF deflector and a dipole magnet acting as an energy spectrometer. The longitudinal current distribution of the electron bunch traveling through the PolariX TDS is first mapped linearly to a transverse one using the X-band RF deflector. The electron bunch is then energetically dispersed by the dipole magnet. If the TDS streak direction and the dipole bending direction are perpendicular, this setup allows for mapping of the longitudinal phase-space density, thereby enhancing the operational capabilities for optimizing the longitudinal bunch parameters that are crucial for the FEL process [13]. As the TDS is installed downstream of the undulators, it measures the phase space after the SASE process has created intense XUV pulses. This has two important consequences, namely, that one can indeed monitor with the TDS exactly the same FEL pulse that is detected with the THz streaking (for SASE every pulse is different) and by analyzing the TDS trace, one can reconstruct which part of the electron pulse was actually lasing.

In the lasing part, the electrons lose energy (which is transferred into the XUV pulse) and the energy spread increases. Figure 2a,b show images acquired by PolariX TDS for a single electron pulse. Especially in Figure 2a, one can see in the center part that the energy distribution is much wider compared to the ends, indicating the enhanced energy spread and the electrons in this part have less energy. By analyzing the image in detail and comparing it to a reference where no SASE process took place, it is possible to infer the shape of the ultrashort XUV photon pulses [15]. Here, we only concentrate on the determination of the lasing part of the electron bunch.

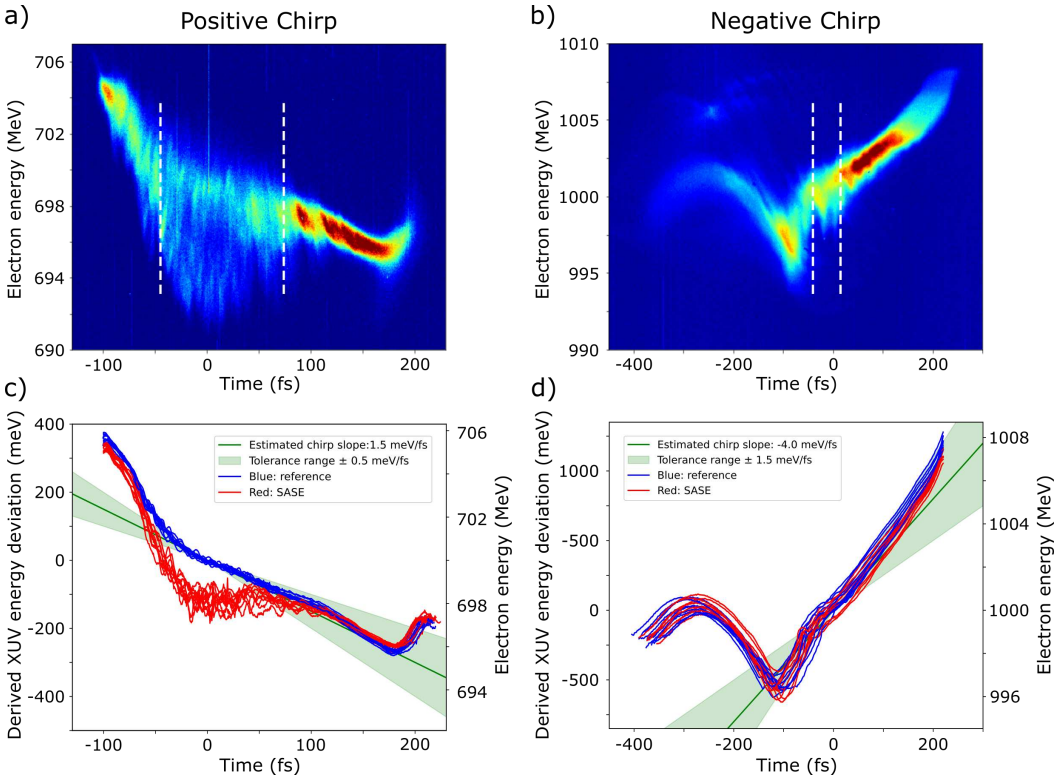

Figure 2. (**a**) A single-shot longitudinal phase space image measured with PolariX, showing a positive energy chirp (low-energy electrons are at the head of the bunch and high-energy electrons are at the tail) on the electron bunch. The white dashed lines show the lasing range on the bunch. (**b**) A single-shot longitudinal phase space image measured with PolariX, showing a negative energy chirp on the electron bunch. (**c**) Computed center of gravity of the phase space images for several images of the FEL setting shown in (**a**). Lasing-on (red) as well as lasing-off (blue) condition is shown. Lasing took place in the ranges where the red and blue curves deviate. The energy chirp of the electron bunch is calculated from a large number of lasing-off measurements and the averaged value is shown as a green line. The green shaded area ("fluctuation range") indicates the variation of the linear fits. (**d**) Center of gravity analyzed for the phase space images with negative chirp as exemplary shown in (**b**). Here, the lasing was rather weak, leading to only a small modulation of the electron bunch. In addition for this setting we find a much larger variation of the slopes fitted to the lasing part as compared to the positive setting.

The effect of an energy chirp on the SASE FEL operation was studied in [29,30], where the so-called energy chirp parameter was introduced. When this parameter is large, it can significantly suppress the FEL gain and should be compensated by a linear undulator taper [30]. In our experiments, the chirp parameter was relatively small, so that the effect on the FEL gain was weak, therefore, no chirp-taper compensation was necessary. The only essential effect of the chirp in the electron beam was photon pulse chirping. For constant undulator settings, the electron energy directly determines the wavelength λ of the FEL pulse as

$$\lambda \propto \frac{1}{\gamma^2}, \tag{3}$$

with the relativistic γ factor representing the electron energy [31].

As the electron pulse energy distribution is strongly modified by the SASE process (at least for XUV pulse energies exceeding 100 µJ), it is difficult to determine an energy chirp from the lasing pulse. Thus, one needs to look at the electron pulse before the lasing sets in to obtain a reliable energy distribution of the electron bunch, influencing the wavelength distribution of the XUV pulse and, thus, determining the chirp. To suppress lasing, a steerer magnet in front of the undulator section is used to slightly deviate the electron bunch

from the lasing trajectory, thus prohibiting lasing but not significantly altering the overall energy distribution.

Figure 2c,d show the center of gravity of the electron bunch calculated from the TDS images for lasing-on and lasing-off conditions. Each red curve represents the center of gravity of a lasing electron bunch with a setup similar to the one shown in Figure 2a,b. The blue curve represents the center of gravity of a non-lasing electron bunch measured separately.

The linear energy chirp of the electron bunch is determined from the lasing-off center of gravity curves by linearly fitting the range where the lasing takes place. Using the independently measured central wavelengths of the XUV pulses and the scaling of Equation (3), we can map the electron energy chirp (in meV/fs, right axis in Figure 2c,d) to the XUV frequency chirp expressed in meV/fs (left axis). The green line in Figure 2c,d shows the mean value of the linear fits from a large number of analyzed shots, quantifying the electron bunch's initial energy chirp. The green shaded area, referred to as the "fluctuation range" shows the spread of slopes taken from the linear fits.

Ad the PolariX results are also influenced by the spatial distribution of the electron bunch, two measurements of opposing streaking field were conducted and the determined XUV chirp (Figure 3a) is the average of the two measurements. For the presented measurements there were only small differences visible, pointing to a not strongly spatially tilted electron bunch.

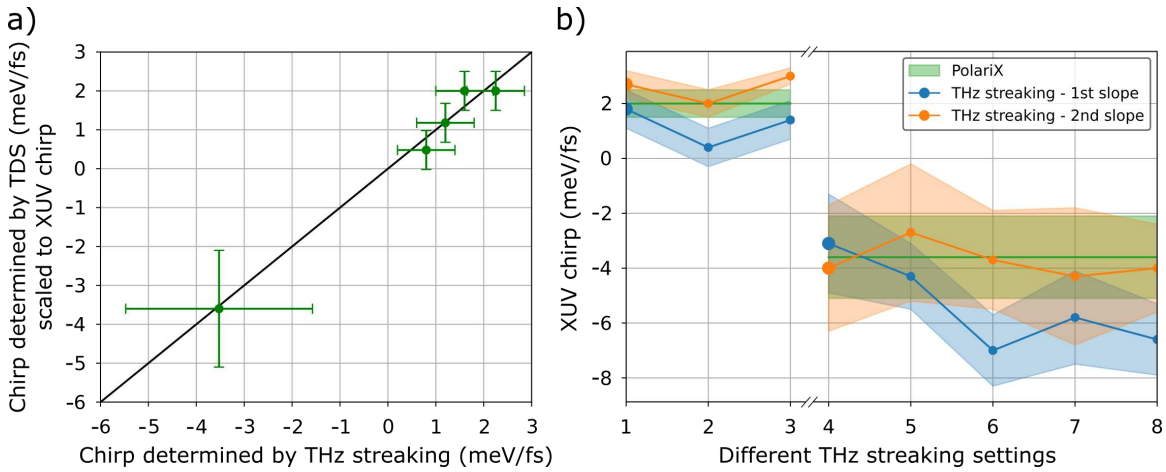

Figure 3. (**a**) Summary of chirp measurements. The linear XUV chirp measured by THz streaking agrees well with the predicted XUV chirp derived from the electron bunch chirp. The shown values are the average and the respective fluctuations of several thousand single shot measurements, simultaneously measured by THz streaking and PolariX TDS. (**b**) Investigation of the influence of the measured chirp values on different settings in the THz streaking setup. The energy resolution of the eTOFs, THz field strength and the number of created photoelectrons were changed significantly. The assignment of the numbers to the different settings is explained in the text. The chirp calculated from TDS data is marked by a green line, with the fluctuation range indicated by a green shade. For the XUV chirp measured using THz streaking, orange denotes the values measured at the second slope and blue, the first slope. Data points 1 and 4 are highlighted with larger points, as they are measured with the standard operation settings of the THz streaking setup. Smaller data points are measured for unfavorable settings.

The next section presents a detailed comparison between the XUV chirp measured using THz streaking and the corresponding XUV chirp calculated from PolariX data. This comparison provides insights into the pros and cons of these measurement techniques.

3. Discussion

The FEL was tuned to several different electron energy chirps with positive as well as negative chirp. For each configuration, single-shot data were acquired simultaneously

using THz streaking and PolariX TDS. To ensure that the XUV chirp measured by THz streaking was independent of the streaking setup parameters, several parameters of the THz detection system were systematically varied, and data were collected for each configuration.

Two different settings of the accelerator were used to cover a larger range for the measurements. Firstly, FLASH2 was operated at an electron bunch energy of ∼1.0 GeV and an electron bunch charge of ∼0.20 nC. This resulted in XUV pulses with ∼16 nm (77 eV) and a pulse duration of ∼80 fs with ∼40 µJ average per FEL pulse for the negative chirp and ∼180 fs with ∼300 µJ for the positive chirp. Secondly, FLASH2 had an electron bunch energy of ∼0.7 GeV and the electron bunch charge was set to 0.26 nC. This configuration resulted in XUV pulses at ∼28 nm (44 eV) with pulse durations around 120 fs and ∼140 µJ pulse energy.

In order to generate a positive chirp (low-energy electrons were at the head of the bunch and high-energy electrons were at the tail), the initially strongly positively chirped electron pulse is under-compressed in magnetic chicanes. To obtain a negative chirp, we had to go to the over-compression regime. We tried to linearize the longitudinal phase space by compensating nonlinearities due to the RF curvature and collective effects in the FLASH accelerator. As the latter are typically strong at FLASH, perfect compensation was not possible, as one can see in Figure 2b. In principle, the chirp can be made larger than what we used in our measurements by compressing the beam stronger. However, collective effects (especially longitudinal space charge) become too strong adding much larger nonlinearities, and can even reverse the sign of the linear part. In this space-charge-dominated regime, the energy chirp at FLASH can exceed our measurements by one or two orders of magnitude due to the short time scale (few femtoseconds) [32]. This regime, however, cannot be studied with the diagnostics described in this paper.

Figure 3a presents the average values of the chirps including the measured fluctuation range indicated by the error bars. The chirp determined by THz streaking (horizontal axis) ranges from −4 meV/fs to 2 meV/fs, meaning that per fs the central energy de- or increases by few meV. Considering a 2 meV/fs chirp for the 180 fs long XUV pulse at 77 eV photon energy, we obtain an energy change of about 0.36 eV within the FWHM of the pulse. Superimposed with the natural FLASH2 bandwidths of about 0.5% [1], we end up at the measured bandwidth of ∼0.7%. The energy changes of the electrons in the accelerator monitored by PolariX were scaled to the expected changes in the XUV pulse, as described above. Despite the different measurement techniques, we obtained a rather good agreement of the measured chirp values for several different settings of FLASH2. This supports the assumption that both diagnostics can be effectively used to determine the chirp of the XUV SASE pulses, at least in its linear part.

For the two extreme cases of positive and negative chirp, a more detailed investigation was conducted. Here, we looked at the dependence of the chirp determined by the THz streaking on different settings of the THz detection setup without altering the FEL pulse intentionally. The aim was to see how sensitive the results of the THz streaking depend on the specific streaking setting and to what extent we can deviate from optimal streaking conditions and still provide reliable chirp measurements. For all measurements we looked at the "first" as well as the "second" slope of the THz field, as shown in Figure 1b. To alter the streaking conditions, the electron spectrometer resolution, the signal level (including space charge effects), and the THz field strength were changed.

In Figure 3b, the blue data points represent the average XUV chirp measured with photoelectrons streaked by the first slope of the THz field, while orange data points show the average XUV chirp value measured with photoelectrons streaked by the second slope. The blue and orange shaded areas indicate the statistical distribution of the XUV chirp measurements for each streaking setup configuration. The green shaded areas show the XUV chirp derived from the electron bunches using PolariX.

Data point **(1)** was measured with optimum streaking conditions (maximum streaking field, best energy resolution, and optimum signal level). To study the impact of the THz streaking field on the measured XUV chirp, the pulse energy of the laser producing the

THz field was reduced to 50% for the second data point **(2)**. This reduced the streaking speed by only about 6%, as the THz production is operated in the saturation regime. For the third data point **(3)**, the pulse energy of the laser was further reduced to 30%. As a result, the streaking speed was reduced by about 30%. Throughout these measurements, the eTOF resolution (i.e., the retardation voltage) was kept constant. For these points, there is a certain variation of the chirp visible that does not seem to depend systematically on changes in the streaking field. The laser generating the THz field shows only 1% rms pulse energy fluctuations, making the resulting fluctuations in the THz field strength negligible compared with other sources of fluctuation. Therefore, these fluctuations may be attributed to drifts and fluctuations during the measurements (about 20 min per setting).

The data points **(4–8)** show measurements with negative chirp. Point **(4)** denotes again the optimum streaking settings. This setting also shows the best agreement between the values measured on both slopes of the THz streaking and the values determined by the PolariX TDS analysis. As the next step, in point **(5)**, the retardation voltage was reduced (increasing E_{kin} from 36 eV to 44 eV), leading to a worse energy resolution of the eTOF. Here, we see indeed less agreement between the two techniques. Reducing the eTOF resolution even further in point **(6)**, the retardation voltage was reduced even more (increasing E_{kin} from 44 eV to 52 eV); therefore, the broadening of the streaking could not be determined accurately, leading to discrepancies between THz streaking and PolariX. For the seventh point **(7)**, the XUV intensity was reduced to one-fourth, decreasing the number of photoelectrons created by the same amount. Thus, the signal-to-noise ratio decreased and statistical fluctuations increased (see, e.g., [10]). Conversely, for the last point **(8)**, the FEL intensity was increased four times higher, showing already signs of space charge broadening by too many photoelectrons created in the small FEL focal volume (see e.g., [10]).

Looking in more detail at Figure 3b, one can see that the fluctuations of the measured chirp differ significantly for different FEL settings. For the negative chirp setting, the SASE level was significantly lower and the electron bunch distribution was much more fluctuating, as shown in Figure 2b, leading to a broader distribution of possible chirp values determined by the TDS analysis. We also see much larger fluctuations in the chirp determined by the THz streaking and, thus, we attribute this mainly to a more unstable electron bunch, as in the positive chirp case. Still, there is a second reason why the chirp values measured by THz streaking show a larger variation. The pulse duration measured at this setting was shorter than the positive chirp case, leading to less broadening in the streaking process and thus the difference between eTOF1 and eTOF2 broadening was less, making it harder to determine the chirp accurately. The measurement at the second slope showed an even broader distribution compared with those with the first slope. This could be attributed to the even lower streaking speed (and thus broadening) of the second compared with the first slope.

For the negative chirp setting, one can see in Figure 3b that the first slope of the streaking field showed a much larger sensitivity to the changes in the streaking setup, while the data from the second slope show a broader distribution but are less sensitive to changes in the setup settings. Up until now, we do not have a solid explanation why the chirp determined for worse streaking conditions on the first slope predicts systematically higher chirps than were present.

Comparing the measurements and data analysis of both techniques, we can explore their specific strengths and drawbacks. An essential difference is that THz streaking measures the actual XUV pulse directly, while PolariX needs a prior assumption about where the lasing occurs within the electron bunch, which is particularly difficult for low-energy pulses where the lasing part within the bunch is uncertain or in cases where different parts of the electron bunch contribute to the lasing. Here, a detailed analysis of the PolariX analysis is needed while THz streaking delivers electron spectra reliably for XUV pulse energies of only ∼1 µJ [10,24]. In addition, Figure 3b shows that even with significantly detuned measurement parameters, the THz streaking technique is still able to reliably

determine both the sign and an approximate value of the chirp. Additionally, THz streaking has the advantage of being able to measure pulse duration parasitically [24], while PolariX requires separate lasing-off measurements, disrupting regular beam operations from time to time.

One limitation of THz streaking is that it can only determine the linear part of the chirp of XUV pulses reliably with the used approach (Equation (2)). Higher orders would alter not only the pulse widths, but also the pulse shape, but within current signal to noise limits an explicit quantitative calculation of higher order contributions is not possible. Still, in principle, complex electron bunch distributions with nonlinear chirp contributions can be tuned at FLASH. For instance, as illustrated in Figure 2b, if the lasing part of the bunch would be larger, strong second and third-order contributions would be present, leading to negative as well as positive chirped parts in one electron bunch. In such a case, THz streaking would lead to incorrect results. Thus, ideally, the combination of both techniques is preferable to ensure a reliable analysis.

Generally, THz streaking based on $LiNbO_3$ as the THz source has a limited range for measuring pulse durations [10]. The typical range in which the pulse duration can be determined with standard analysis is about 30–300 fs (FWHM) for unchirped pulses. For chirped pulses, accurately determining the difference in streaking width requires an even smaller range. Also, the ability to measure XUV pulses below about 30 fs with PolariX is difficult. To overcome these limitations, the future planning for FLASH2 is to rely on the determination of the XUV chirp for pulses longer ∼30 fs using PolariX, while for shorter pulses, a new type streaking setup will be implemented based on angular streaking [33,34]. This technique can not only determine the pulse duration in the range of ∼30 fs down to the sub fs range, but in addition offers the option to even measure higher-order chirps. By developing and integrating angular streaking techniques into existing FEL facilities, researchers can significantly enhance the precision and control of XUV pulses, leading to more accurate and comprehensive studies of ultrafast phenomena.

4. Conclusions

The frequency chirp of SASE-based free-electron laser XUV pulses at FLASH2 was measured using two entirely different approaches. THz streaking determines the linear chirp of the XUV pulses directly, while the PolariX TDS monitors the phase space of the electrons in the accelerator that produced the XUV radiation. Using simple scaling laws, the XUV chirp can be derived this way as well. Our results show a good agreement between the two methods across a large range of chirp values, including negative as well as positive chirps. In addition, THz streaking seems rather robust against significantly detuned experimental parameters.

Analysis of several years of THz streaking data revealed that XUV pulses often exhibit a remaining chirp, either negative or positive. This highlights the importance of chirp monitoring, especially for experiments sensitive to chirp. Future work will focus on extending these techniques to characterize even shorter pulses and higher-order chirp.

Author Contributions: Measurements, M.M.B., G.G., S.D., E.A.S., I.J.B.M., R.I. and N.M.; writing—original draft preparation, M.M.B. and S.D.; writing—review and editing, M.M.B., S.D., G.G. and E.A.S. All authors have read and agreed to the published version of the manuscript.

Funding: This research was funded by Deutsche Forschungsgemeinschaft (DFG, German Research Foundation) grant number 491245950.

Institutional Review Board Statement: Not applicable.

Informed Consent Statement: Not applicable.

Data Availability Statement: The data presented in this study are available on request from the corresponding authors.

Acknowledgments: We acknowledge DESY (Hamburg, Germany), a member of the Helmholtz Association HGF, for providing the experimental facilities and the financial support necessary to

carry out this research. We also want to acknowledge the work of the scientific and technical team at FLASH, in particular Mathias Vogt and Juliane Rönsch-Schulenburg for helpful discussions and for fulfilling our special wishes during our beamtimes. We also like to thank Ulrike Frühling for useful discussions and suggestions for improving this article.

Conflicts of Interest: The authors declare no conflicts of interest.

References

1. Ackermann, W.; Asova, G.; Ayvazyan, V.; Azima, A.; Baboi, N.; Bähr, J.; Balandin, V.; Beutner, B.; Brandt, A.; Bolzmann, A.; et al. Operation of a free-electron laser from the extreme ultraviolet to the water window. *Nat. Photonics* **2007**, *1*, 336–342. [CrossRef]
2. Emma, P.; Akre, R.; Arthur, J.; Bionta, R.; Bostedt, C.; Bozek, J.; Brachmann, A.; Bucksbaum, P.; Coffee, R.; Decker, F.J.; et al. First lasing and operation of an ångstrom-wavelength free-electron laser. *Nat. Photonics* **2010**, *4*, 641–647. [CrossRef]
3. Ishikawa, T.; Aoyagi, H.; Asaka, T.; Asano, Y.; Azumi, N.; Bizen, T.; Ego, H.; Fukami, K.; Fukui, T.; Furukawa, Y.; et al. A compact X-ray free-electron laser emitting in the sub-ångström region. *Nat. Photonics* **2012**, *6*, 540–544. [CrossRef]
4. Decking, W.; Abeghyan, S.; Abramian, P.; Abramsky, A.; Aguirre, A.; Albrecht, C.; Alou, P.; Altarelli, M.; Altmann, P.; Amyan, K.; et al. A MHz-repetition-rate hard X-ray free-electron laser driven by a superconducting linear accelerator. *Nat. Photonics* **2020**, *14*, 391–397. [CrossRef]
5. Milne, C.J.; Schietinger, T.; Aiba, M.; Alarcon, A.; Alex, J.; Anghel, A.; Arsov, V.; Beard, C.; Beaud, P.; Bettoni, S.; et al. SwissFEL: The Swiss X-ray Free Electron Laser. *Appl. Sci.* **2017**, *7*, 720. [CrossRef]
6. Ko, I.S.; Kang, H.S.; Heo, H.; Kim, C.; Kim, G.; Min, C.K.; Yang, H.; Baek, S.Y.; Choi, H.J.; Mun, G.; et al. Construction and Commissioning of PAL-XFEL Facility. *Appl. Sci.* **2017**, *7*, 479. [CrossRef]
7. Düsterer, S.; Rehders, M.; Al-Shemmary, A.; Behrens, C.; Brenner, G.; Brovko, O.; DellAngela, M.; Drescher, M.; Faatz, B.; Feldhaus, J.; et al. Development of experimental techniques for the characterization of ultrashort photon pulses of extreme ultraviolet free-electron lasers. *Phys. Rev. ST Accel. Beams* **2014**, *17*, 120702. [CrossRef]
8. Frühling, U.; Wieland, M.; Gensch, M.; Gebert, T.; Schütte, B.; Krikunova, M.; Kalms, R.; Budzyn, F.; Grimm, O.; Rossbach, J.; et al. Single-shot terahertz-field-driven X-ray streak camera. *Nat. Photonics* **2009**, *3*, 523–528. [CrossRef]
9. Grguraš, I.; Maier, A.R.; Behrens, C.; Mazza, T.; Kelly, T.J.; Radcliffe, P.; Düsterer, S.; Kazansky, A.K.; Kabachnik, N.M.; Tschentscher, T.; et al. Ultrafast X-ray pulse characterization at free-electron lasers. *Nat. Photonics* **2012**, *6*, 852–857. [CrossRef]
10. Ivanov, R.; Macias, I.J.B.; Liu, J.; Brenner, G.; Roensch-Schulenburg, J.; Kurdi, G.; Frühling, U.; Wenig, K.; Walther, S.; Dimitriou, A.; et al. Single-shot temporal characterization of XUV pulses with duration from ∼10 fs to ∼350 fs at FLASH. *J. Phys. B At. Mol. Opt. Phys.* **2020**, *53*, 184004. [CrossRef]
11. Frühling, U. Light-field streaking for FELs. *J. Phys. B At. Mol. Opt. Phys.* **2011**, *44*, 243001. [CrossRef]
12. Azima, A.; Bödewadt, J.; Becker, O.; Düsterer, S.; Ekanayake, N.; Ivanov, R.; Kazemi, M.M.; Lazzarino, L.L.; Lechner, C.; Maltezopoulos, T.; et al. Direct measurement of the pulse duration and frequency chirp of seeded XUV free electron laser pulses. *New J. Phys.* **2018**, *20*, 013010. [CrossRef]
13. Craievich, P.; Bopp, M.; Braun, H.H.; Citterio, A.; Fortunati, R.; Ganter, R.; Kleeb, T.; Marcellini, F.; Pedrozzi, M.; Prat, E.; et al. Novel *X*-band transverse deflection structure with variable polarization. *Phys. Rev. Accel. Beams* **2020**, *23*, 112001. [CrossRef]
14. Marchetti, B.; Grudiev, A.; Craievich, P.; Assmann, R.; Braun, H.H.; Catalan Lasheras, N.; Christie, F.; D'Arcy, R.; Fortunati, R.; Ganter, R.; et al. Experimental demonstration of novel beam characterization using a polarizable X-band transverse deflection structure. *Sci. Rep.* **2021**, *11*, 3560. [CrossRef] [PubMed]
15. Behrens, C.; Decker, F.J.; Ding, Y.; Dolgashev, V.A.; Frisch, J.; Huang, Z.; Krejcik, P.; Loos, H.; Lutman, A.; Maxwell, T.J.; et al. Few-femtosecond time-resolved measurements of X-ray free-electron lasers. *Nat. Commun.* **2014**, *5*, 3762. [CrossRef]
16. Zewail, A.H. Femtochemistry. Past, present, and future. *Pure Appl. Chem.* **2000**, *72*, 2219–2231. [CrossRef]
17. Brixner, T.; Gerber, G. Quantum Control of Gas-Phase and Liquid-Phase Femtochemistry. *ChemPhysChem* **2003**, *4*, 418–438. [CrossRef]
18. Gühr, M.; Ibrahim, H.; Schwentner, N. Controlling vibrational wave packet revivals in condensed phase: Dispersion and coherence for Br_2 in solid Ar. *Phys. Chem. Chem. Phys.* **2004**, *6*, 5353–5361. [CrossRef]
19. Ding, T.; Rebholz, M.; Aufleger, L.; Hartmann, M.; Stooß, V.; Magunia, A.; Birk, P.; Borisova, G.D.; Wachs, D.; da Costa Castanheira, C.; et al. Measuring the frequency chirp of extreme-ultraviolet free-electron laser pulses by transient absorption spectroscopy. *Nat. Commun.* **2021**, *12*, 643. [CrossRef]
20. Patterson, B.D.; Abela, R.; Braun, H.H.; Flechsig, U.; Ganter, R.; Kim, Y.; Kirk, E.; Oppelt, A.; Pedrozzi, M.; Reiche, S.; et al. Coherent science at the SwissFEL X-ray laser. *New J. Phys.* **2010**, *12*, 035012. [CrossRef]
21. Ding, T.; Rebholz, M.; Aufleger, L.; Hartmann, M.; Stooß, V.; Magunia, A.; Birk, P.; Borisova, G.D.; da Costa Castanheira, C.; Rupprecht, P.; et al. XUV pump–XUV probe transient absorption spectroscopy at FELs. *Faraday Discuss.* **2021**, *228*, 519–536. [CrossRef] [PubMed]
22. Dejoie, C.; McCusker, L.B.; Baerlocher, C.; Abela, R.; Patterson, B.D.; Kunz, M.; Tamura, N. Using a non-monochromatic microbeam for serial snapshot crystallography. *J. Appl. Crystallogr.* **2013**, *46*, 791–794. [CrossRef]

23. Faatz, B.; Plönjes, E.; Ackermann, S.; Agababyan, A.; Asgekar, V.; Ayvazyan, V.; Baark, S.; Baboi, N.; Balandin, V.; von Bargen, N.; et al. Simultaneous operation of two soft x-ray free-electron lasers driven by one linear accelerator. *New J. Phys.* **2016**, *18*, 062002. [CrossRef]
24. Ivanov, R.; Bidhendi, M.M.; Macias, I.J.B.; Macias, I.J.B.; Brachmanski, M.; Kreis, S.; Bonfigt, S.; Degenhardt, M.; Czwalinna, M.K.; Pergament, M.; et al. Free-electron laser temporal diagnostic beamline FL21 at FLASH. *Opt. Express* **2023**, *31*, 19146–19158. [CrossRef] [PubMed]
25. Ivanov, R.; Liu, J.; Brenner, G.; Brachmanski, M.; Düsterer, S. FLASH free-electron laser single-shot temporal diagnostic: terahertz-field-driven streaking. *J. Synchrotron Radiat.* **2018**, *25*, 26–31. [CrossRef] [PubMed]
26. Oelze, T.; Kulyk, O.; Schütte, B.; Frühling, U.; Frühling, U.; Klimešová, E.; Jagielski, B.; Dittrich, L.; Drescher, M.; Drescher, M.; et al. THz streak camera performance for single-shot characterization of XUV pulses with complex temporal structures. *Opt. Express* **2020**, *28*, 20686–20703. [CrossRef]
27. Christie, F.; Rönsch-Schulenburg, J.; Vogt, M. A PolariX TDS for the FLASH2 Beamline. In Proceedings of the 39th International Free Electron Laser Conference (FEL2019), Hamburg, Germany, 26–30 August 2019; pp. 328–331. [CrossRef]
28. Craievich, P.; Aßmann, R.; Bopp, M.; Braun, H.H.; Lasheras, N.C.; Christie, F.; Citterio, A.; D'Arcy, R.; Dorda, U.; Foese, M.; et al. The PolariX-TDS Project: Bead-Pull Measurements and High-Power Test on the Prototype. In Proceedings of the 39th International Free Electron Laser Conference (FEL2019), Hamburg, Germany, 26–30 August 2019; pp. 396–399. [CrossRef]
29. Krinsky, S.; Huang, Z. Frequency chirped self-amplified spontaneous-emission free-electron lasers. *Phys. Rev. Spec. Top. Accel. Beams* **2003**, *6*, 050702. [CrossRef]
30. Saldin, E.L.; Schneidmiller, E.A.; Yurkov, M.V. Self-amplified spontaneous emission FEL with energy-chirped electron beam and its application for generation of attosecond x-ray pulses. *Phys. Rev. Spec. Top. Accel. Beams* **2006**, *9*, 050702. [CrossRef]
31. Saldin, E.L.; Schneidmiller, E.A.; Yurkov, M.V. *The Physics of Free Electron Lasers*; Springer: Berlin/Heidelberg, Germany, 2000.
32. Schneidmiller, E.; Dreimann, M.; Kuhlmann, M.; Rönsch-Schulenburg, J.; Zacharias, H. Generation of Ultrashort Pulses in XUV and X-ray FELs via an Excessive Reverse Undulator Taper. *Photonics* **2023**, *10*, 653. [CrossRef]
33. Hartmann, N.; Hartmann, G.; Heider, R.; Wagner, M.S.; Ilchen, M.; Buck, J.; Lindahl, A.O.; Benko, C.; Grünert, J.; Krzywinski, J.; et al. Attosecond time–energy structure of X-ray free-electron laser pulses. *Nat. Photonics* **2018**, *12*, 215–220. [CrossRef]
34. Heider, R.; Wagner, M.S.; Hartmann, N.; Ilchen, M.; Buck, J.; Hartmann, G.; Shirvanyan, V.; Lindahl, A.O.; Grünert, J.; Krzywinski, J.; et al. Megahertz-compatible angular streaking with few-femtosecond resolution at x-ray free-electron lasers. *Phys. Rev. A* **2019**, *100*, 053420. [CrossRef]